JACS
JOURNAL OF THE AMERICAN CHEMICAL SOCIETY

Article

pubs.acs.org/JACS

Stable Covalent Organic Frameworks for Exceptional Mercury Removal from Aqueous Solutions

Ning Huang, Lipeng Zhai, Hong Xu, and Donglin Jiang*

Field of Environment and Energy, School of Materials Science, Japan Advanced Institute of Science and Technology, 1-1 Asahidai, Nomi 923-1292, Japan

Supporting Information

ABSTRACT: The pre-designable porous structures found in covalent organic frameworks (COFs) render them attractive as a molecular platform for addressing environmental issues such as removal of toxic heavy metal ions from water. However, a rational structural design of COFs in this aspect has not been explored. Here we report the rational design of stable COFs for Hg(II) removal through elaborate structural design and control over skeleton, pore size, and pore walls. The resulting framework is stable under strong acid and base conditions, possesses high surface area, has large mesopores, and contains dense sulfide functional termini on the pore walls. These structural features work together in removing Hg(II) from water and achieve a benchmark system that combines capacity, efficiency, effectivity, applicability, selectivity, and reusability. These results suggest that COFs offer a powerful platform for tailor-made structural design to cope with various types of pollution.

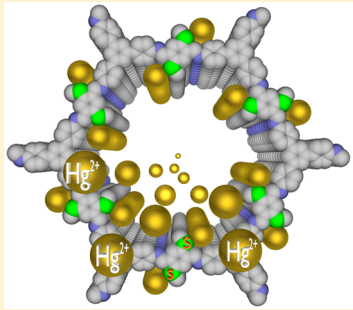

INTRODUCTION

Covalent organic frameworks (COFs) enable precise integration of organic building blocks into pre-designable porous skeletons through topology design.[1] Progress over the past decade in the exploration of topology diagrams and synthetic reactions has developed a variety of COFs[1−9] with unique functions, such as semiconducting,[4] emission,[5] catalysis,[6] proton conduction,[7] and energy conversion and storage.[8] Owing to the structural diversity of skeletons and pore walls, COFs offer a platform for designing high-performance materials that are promising for addressing environmental issues. However, exploration of COFs to challenge environmental issues has been rarely pursued.[9]

As a great threat to public health and the environment, Hg(II) pollution causes serious damage to human beings, known as Minamata disease.[10] In this context, removal of Hg(II) from polluted water to a concentration as low as possible is an important issue. Compared to traditional chemical reaction methods, adsorption using porous adsorbents is much superior because of its simplicity and cost efficiency.[10] In addition to removal capacity, efficiency, and effectivity, suitable porous materials must be stable in water over a wide pH range (1−14) and must be reusable.[10c] Traditional porous materials, including clays, activated carbons, and zeolites, usually have limited capacity.[10d−f] Amorphous porous organic polymers are potential candidates, but they lack principles for molecular design and methods for structural control.[10g] Although metal−organic frameworks (MOFs) have been developed for Hg(II) removal based on their high surface areas, stable performance in aqueous solutions remains a challenging.[11a,b] A very first try using COFs is based on a long alkyl sulfide functionalized COF, i.e., COF-LZU8, which is useful for sensing Hg(II) owing to the fluorescence quenching of COF by Hg(II);[11c] however, its limited capacity and stability preclude any implementation. Therefore, a porous material that meets the requirements of capacity, stability, and reusability remains a challenge in chemistry.

In response to the harsh requirements for Hg(II) removal from aqueous solutions, we rationally designed and synthesized a suitable COF structure. First, for the stability, we have developed an extremely stable COF based on an imine-linked skeleton,[6b] by integrating resonance effects (methyl sulfide units) to the phenyl edges, which is stable in aqueous solutions over a wide pH range. Second, for the capacity, efficiency, and effectiveness, we introduced the shortest sulfide functional chains and developed two-dimensional (2D) COFs that enable the highest packing of sheets to achieve the highest sulfur content. The shortest sulfide chains on the pore walls suppress chain entanglement, help to expose the active sulfur sites to Hg(II), and endow the COFs with retained large pores, high surface area, and large pore volume. Finally, for the reusability, the methyl sulfide units are much more stable against oxygen oxidation compared to thiol units; this functionality enables stable cycle performance. Herein, we report the newly designed imine-linked stable COF with thioether units on the pore walls to remove Hg(II) from water based on the well-established Hg(II)-thioether ligation chemistry; the thioether group forms a Hg−S coordination bond with a binding energy of 117 kJ mol^{-1}.[11d]

MATERIALS AND METHODS

1,3,5-Trimethylbenzene (Mesitylene), *o*-dichlorobenzene (*o*-DCB), 1-butanol (*n*-BuOH), acetone, chloroform ($CHCl_3$), tetrahydrofuran

Received: November 30, 2016
Published: January 25, 2017

DOI: 10.1021/jacs.6b12328
J. Am. Chem. Soc. 2017, 139, 2428−2434

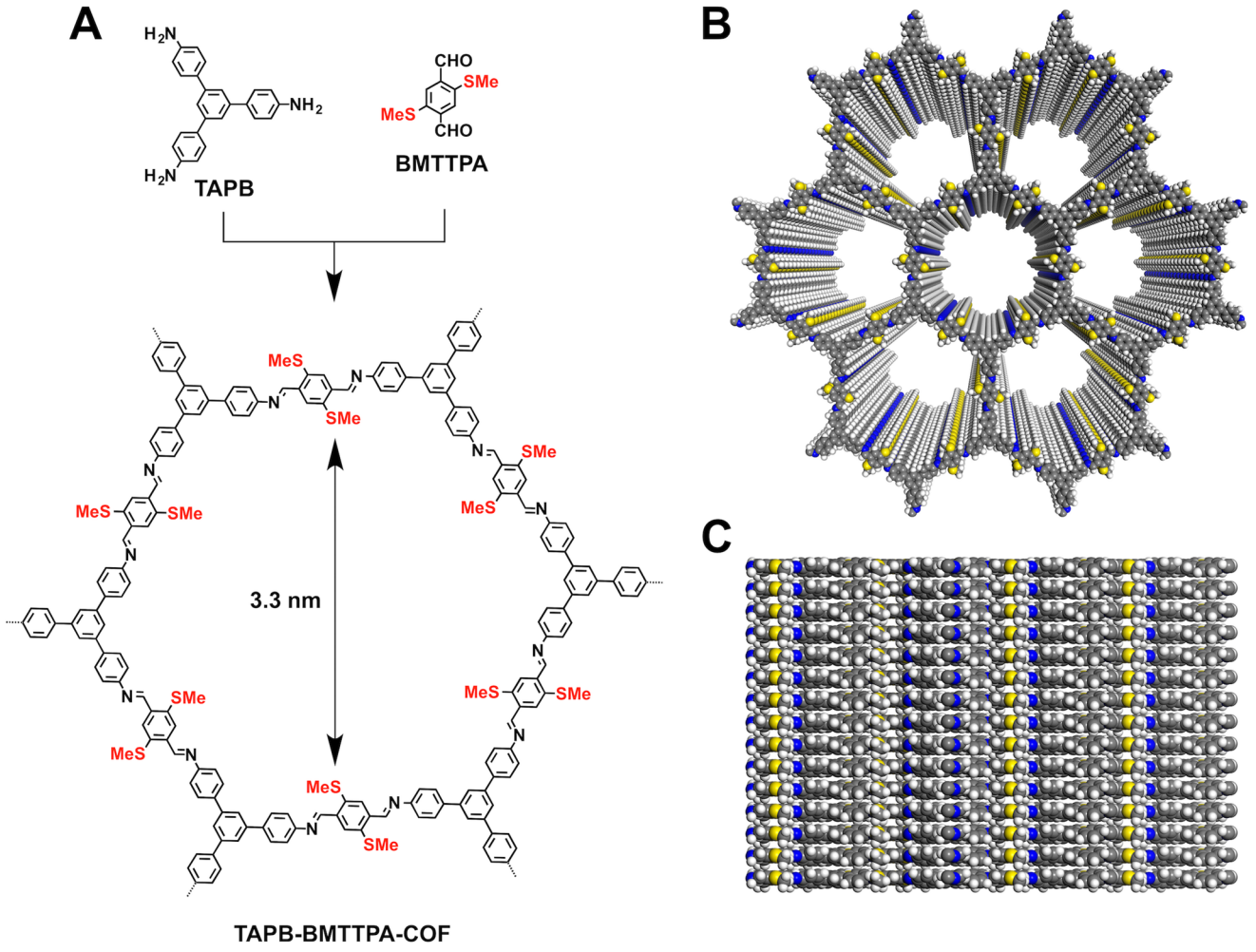

Figure 1. (A) Schematic of the synthesis of TAPB-BMTTPA-COF via the condensation of TAPB and BMTTPA. (B) Top and (C) side views of TAPB-BMTTPA-COF (yellow, S; blue, N; gray, C; white, hydrogen).

(THF), and 1,4-dioxane were purchased from Kanto Chemicals. 1,3,5-Tris(4-aminophenyl)benzene (TAPB), potassium carbonate (K_2CO_3), and anhydrous hydrazine were purchased from Tokyo Kasai Co. (TCI). 2,5-Bis(methylthio)terephthalaldehyde (BMTTPA) was synthesized according to the previous literature.[12] An *o*-DCB/BuOH/6 M AcOH (5/5/1 by vol.; 1.1 mL) mixture of TAPB (0.02 mmol, 7.02 mg) and BMTTPA (0.03 mmol, 15.3 mg) in a Pyrex tube (10 mL) was degassed by three freeze−pump−thaw cycles. The tube was sealed off and heated at 120 °C for 3 days. The precipitate was collected by centrifugation and washed with anhydrous THF five times and acetone twice. The powder was dried at 120 °C under vacuum overnight to yield the TAPB-BMTTPA-COF in an isolated yield of 84%.

Molecular modeling and Pawley refinement were carried out using Reflex, a software package for crystal determination from XRD patterns, implemented in MS modeling version 4.4 (Accelrys Inc.). Unit cell dimension was first manually determined from the observed XRD peak positions using the coordinates. We performed Pawley refinement to optimize the lattice parameters iteratively until the R_{WP} value converges. The pseudo-Voigt profile function was used for whole profile fitting, and the Berrar−Baldinozzi function was used for asymmetry correction during the refinement processes.

The efficiency of TAPB-BMTTPA-COF as mercury adsorbent for capturing Hg(II) from aqueous solutions has been examined by investigating the mercury adsorption kinetics of TAPB-BMTTPA-COF (25.0 mg) in 10 ppm solution (pH = 7.0) of $Hg(NO_3)_2$ (50.0 mL). The experimental results were fitted with the pseudo-second-order kinetic model using the equation of $t/q_t = 1/(k_2 q_e^2) + t/q_e$, where k_2 (g mg^{-1} min^{-1}) is the rate constant of pseudo-second-order adsorption, q_t (mg g^{-1}) is the amount of Hg(II) adsorbed at time t (min), and q_e (mg g^{-1}) is the amount of Hg(II) adsorbed at equilibrium.

One measure of a sorbent's affinity for a target metal ion is the distribution coefficient (K_d) measurement. The distribution coefficient is defined as $K_d = (C_i - C_f)V/C_f m$, where C_i is the initial metal ion concentration, C_f is the final equilibrium metal ion concentration, V is the volume of the solution (mL), and m is the mass of sorbent (g). K_d represents an important aspect of any sorbent's performance metrics of metal ion adsorption, and K_d values of 1.0×10^5 mL g^{-1} are usually considered excellent.

RESULTS AND DISCUSSION

Synthesis and Characterization. We developed TAPB as knot and BMTTPA as linker for the preparation of the hexagonal TAPB-BMTTPA-COF (Figure 1A). The condensation reactions were conducted under solvothermal conditions in a mixed solvent of n-butanol and *o*-dicholorobenzene in the presence of acetic acid catalyst at 120 °C for 3 days (Supporting Information (SI)). TAPB-BMTTPA-COF was obtained as a yellow powder in 84% isolation yield and characterized using various methods (Figures S1−S6; Tables S1−S5). TAPB-BMTTPA-COF consists of ordered mesoporous 1D channels and methyl sulfide units on the walls as active sites to anchor Hg(II) (Figure 1B, C). The COF exhibited a stretching vibration band at 1622 cm^{-1} that was assigned to the C═N

DOI: 10.1021/jacs.6b12328
J. Am. Chem. Soc. 2017, 139, 2428−2434

bond (Figure S1). Elemental analysis and energy-dispersive X-ray spectrometry corroborate well with the theoretical values of infinite 2D sheet; the sulfur content was 15.5 wt%, which was the highest among COFs and MOFs (Tables S1 and S2, Figures S2 and S3). Field emission scanning electron microscopy revealed belt morphology (Figure S4). High-resolution transmission electron microscopy showed a layered structure of parallel 2D sheets (Figure S5). Thermal gravimetric analysis demonstrated that TAPB-BMTTPA-COF is stable up to 400 °C under N_2 (Figure S6).

Crystal Structure Resolutions. The crystalline structure of TAPB-BMTTPA-COF was resolved using powder X-ray diffraction (PXRD) in conjunction with computational structural simulations and Pawley refinement. TAPB-BMTTPA-COF exhibited a set of strong PXRD peaks at 2.74°, 4.82°, 5.58°, 7.40°, 9.72°, and 25.42°, which were assigned to the (100), (110), (200), (210), (220), and (001) facets, respectively (Figure 2A, red curve). The Pawley refinement yielded a PXRD pattern (Figure 2A, black curve, Table S3) that is in good agreement with the experimentally observed pattern, as evident by their negligible difference and very low R_{WP} and R_P values of 6.19% and 3.42% (brown curve). Using the density-functional tight-binding (DFTB+) method including Lennard-Jones (LJ) dispersion, the AA stacking mode (Figure 2B) can reproduce the PXRD pattern (Figure 2A, blue curve). A hexagonal unit cell (P6) with the parameters of $a = b = 37.1634$ Å, $c = 3.7794$ Å, $\alpha = \beta = 90°$, and $\gamma = 120°$ (Table S4) was deduced. The presence of the (001) facet at 25.42° corresponds to a $\pi-\pi$ stacking distance of 3.6 Å, indicating that the structural ordering extends along the stacking direction perpendicular to the 2D layers. By contrast, the AB stacking mode (Figure 2C) resulted in small pores covered by neighboring layers and a PXRD pattern (Figure 2A, purple curve, Table S5) that largely deviates from that of the experimentally observed profile.

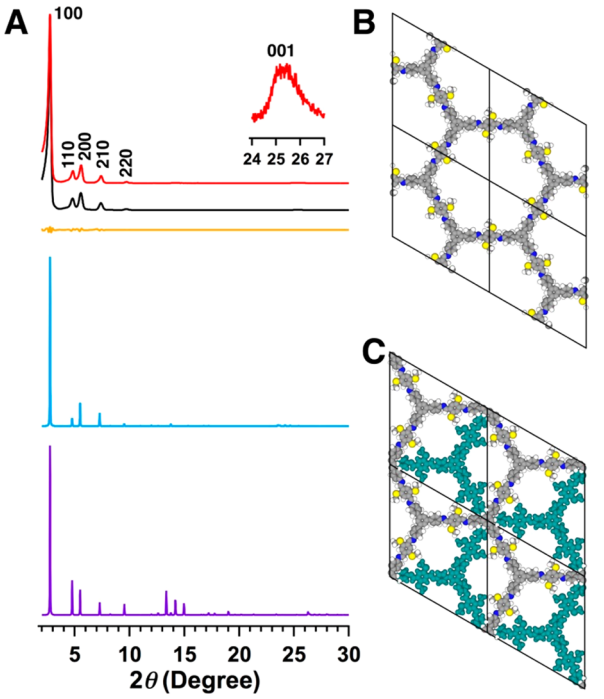

Figure 2. (A) PXRD profiles of TAPB-BMTTPA-COF of the experimentally observed (red), Pawley refined (black) and their difference (orange), simulated using the AA (blue) and staggered AB (purple) stacking modes. Unit cells of (B) the AA and (C) AB stacking modes.

Porosity. The porosity was investigated by using nitrogen sorption isotherm measurements at 77 K. The sorption curve is a typical type IV isotherm (Figure 3A), which is characteristic of mesoporous materials. The Brunauer–Emmett–Teller (BET) surface area and pore volume were estimated to be 1934 $m^2\ g^{-1}$ and 1.03 $cm^3\ g^{-1}$, respectively. The pore size distribution calculated by using the nonlocal density functional theory (NLDFT) method resulted in a pore size of 3.2 nm (Figure 3B), which is the same as the theoretical one. Notably, these surface area and pore volume are much higher than those of any other thiol- or sulfide-modified porous materials.[11]

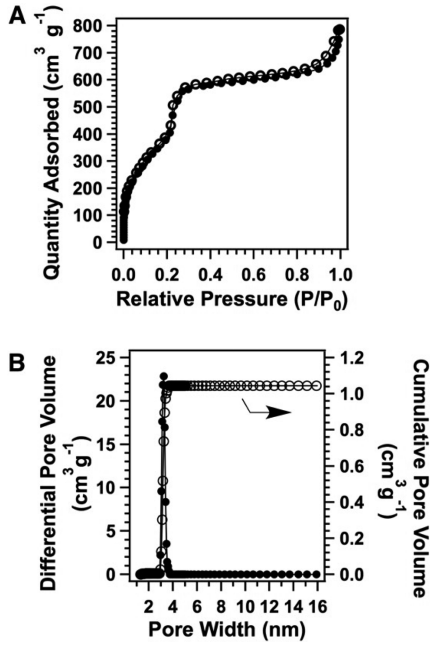

Figure 3. (A) Nitrogen sorption isotherm curves of TAPB-BMTTPA-COF measured at 77 K. (B) Pore volume and pore-size distribution profiles.

Chemical Stability. To investigate the chemical stability, we dispersed the COF samples in different solutions, including boiling water and aqueous HCl (6 M) and NaOH (6 M) solutions, at 25 °C for 3 days. Surprisingly, all the samples exhibited intense PXRD patterns without change in the peak position and intensity, indicating that the high crystallinity is retained under these harsh conditions (Figure 4A). After treatment of these solutions, the COF samples were separated by filtration, and rinsed with water and THF. All the COF samples were then activated at 120 °C under vacuum for 24 h. Notably, the BET surface areas were retained well under these conditions (Figure 4B,C). The resonance effect of methyl sulfide units on the phenyl edges softens the C═N bond polarization-induced repulsions between layers and enhances the stability.[6b]

Hg(II) Capture. In order to investigate the Hg(II) removal capacity, which is a key index for the performance criterion, adsorption isotherm for Hg(II) capture from water was collected by using inductively coupled plasma analysis (SI). The equilibrium adsorption isotherms were well fitted with Langmuir model that yielded a high correlation coefficient (R_2

DOI: 10.1021/jacs.6b12328
J. Am. Chem. Soc. 2017, 139, 2428–2434

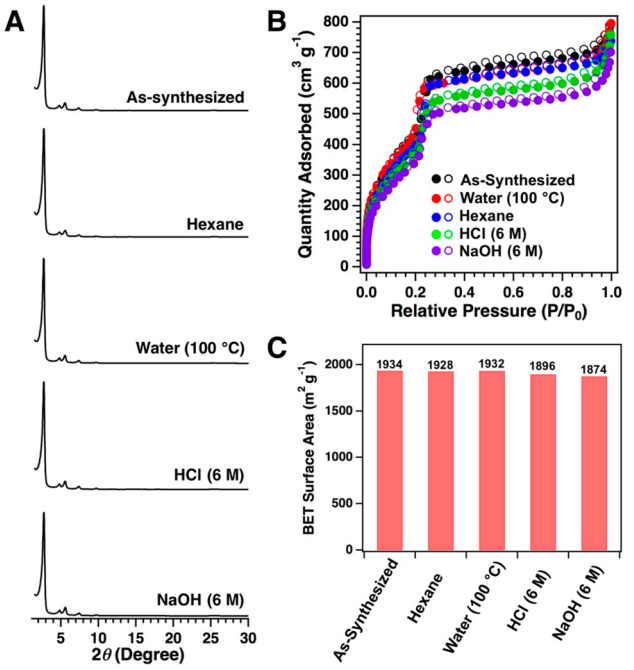

Figure 4. (A) PXRD patterns, (B) N_2 sorption curves, and (C) BET surface areas of the TAPB-BMTTPA-COF samples upon treatment in different solvents.

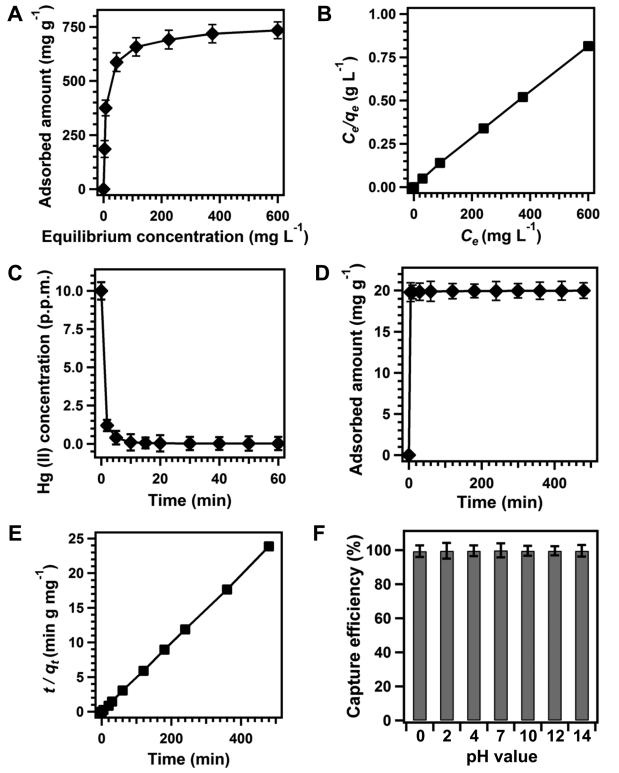

Figure 5. (A) Hg(II) adsorption isotherm at pH = 7 after 12 h. (B) Linear regression by fitting the equilibrium adsorption data with Langmuir adsorption model. (C) Hg(II) sorption kinetics under the initial Hg(II) concentration of 10 ppm and pH = 7. (D) Adsorption curve of Hg(II) versus contact time in aqueous solution at pH = 7. (E) Pseudo-second-order kinetic plot for the adsorption at Hg(II) concentration of 10 ppm and pH = 7. (F) Capture of Hg(II) under different pH conditions after 60 min.

> 0.999) (Figure 5A,B). Surprisingly, the saturated Hg(II) removal capacity of TAPB-BMTTPA-COF was calculated to be 734 mg g^{-1}. This capacity is equivalent to 76% accessibility of the methyl sulfide groups for the removal of the Hg(II) ions. To the best of our knowledge, this Hg(II) removal capacity is much higher than those of most benchmark porous materials, including MOF Zr-DMBD (197 mg g^{-1}),[11e] Zn(hip)(L)-(DMF)(H_2O),[11f] porous carbon (518 mg g^{-1}),[11g] mesoporous silica (600 mg g^{-1}),[11h] and chalcogel-1 (645 mg g^{-1}).[11i] Remarkably, the capacity of TAPB-BMTTPA-COF is more than 3-fold that of COF-LZU8 (236 mg g^{-1}).[11c] The exceptional capacity stems from the high accessibility of methyl sulfide groups that are uncovered on the pore walls of the highly porous TAPB-BMTTPA-COF, which facilitates to trap Hg(II) ions by the COFs.

In addition to the high capacity, TAPB-BMTTPA-COF is outstanding from the viewpoint of removal effectiveness. The reaction kinetics was investigated for a system with $Hg(NO_3)_2$ (50 mL; 10 ppm, pH = 7) and TAPB-BMTTPA-COF (25 mg) at 25 °C (Figure 5C). Surprisingly, we observed extremely quick removal process, whereas over 99% of Hg(II) ions was removed within 5 min. The purification process completes within 15 min and decreases the Hg(II) concentration from 10 to 0.01 ppm (Figure 5C). By fitting with a pseudo-second-order model, the adsorption rate constant (k_2, SI) was evaluated to be 6.31 g mg^{-1} min^{-1} (Figure 5D,E). Notably, this rate constant is almost 10-fold higher than those of other porous materials under similar conditions.[11] This high-rate performance can be attributed to its surface area and pore size that are both sufficiently large to facilitate the diffusion of Hg(II) ions to the methyl sulfide sites. Distribution coefficient (K_d, SI) is generally used to evaluate a sorbent's affinity for metal ions. The K_d value of TAPB-BMTTPA-COF at 25 °C was calculated to be 7.82 × 10^5 mL g^{-1}, which ranks as one of the top values and competes with those of typical benchmark materials, including Zr-DMBD (9.99 × 10^5 mL g^{-1}),[11e] sulfide-modified mesoporous carbons (6.82 × 10^5 mL g^{-1}),[11g] commercial resins (5.1 × 10^5 mL g^{-1}),[11j] LHMS-1 (6.4 × 10^6 mL g^{-1}),[11k] and PAF-1-SH (5.76 × 10^7 mL g^{-1}).[11l]

For practical use, removal of Hg(II) under harsh conditions, such as extreme pH values, is highly desirable. The chemical stability under various harsh conditions was verified for TAPB-BMTTPA-COF (Figure 4A). This feature is an important advantage over silica- or MOFs-based adsorbents that usually suffer from the loss of structures under harsh conditions.[11a,b] Indeed, we observed that TAPB-BMTTPA-COF retained removal efficiency, whereas the Hg(II) concentrations can be reduced from 10 to 0.05 ppm and 0.02 ppm at the pH values of 0 and 14, respectively (Figure 5F). Generally, the pH values of industrial sewage are between 3 and 4, in which the TAPB-BMTTPA-COF still retained excellent adsorption efficiency (99.7−99.8%, Figure S7). The PXRD patterns revealed that the TAPB-BMTTPA-COF did not change its crystalline structure after adsorption of Hg(II) (Figure S8). Structure instability under harsh conditions and deteriorated capacity over a broad pH range have been barriers for other porous materials.[11a−d] As shown above, these challenging issues can be addressed by designing a stable COF skeleton.

Recycle Use. Cycle performance of porous materials is critical for real applications. Surprisingly, the Hg(II)-captured TAPB-BMTTPA-COF was easily regenerated upon rinse with an aqueous HCl solution (6.0 M), which resulted in 100% demetalation. The regenerated COF was then subjected to the next round Hg(II) removal. Notably, TAPB-BMTTPA-COF

DOI: 10.1021/jacs.6b12328
J. Am. Chem. Soc. 2017, 139, 2428−2434

retained 92% of the original capacity even after six cycles (Figure 6A). This result is much superior to other porous

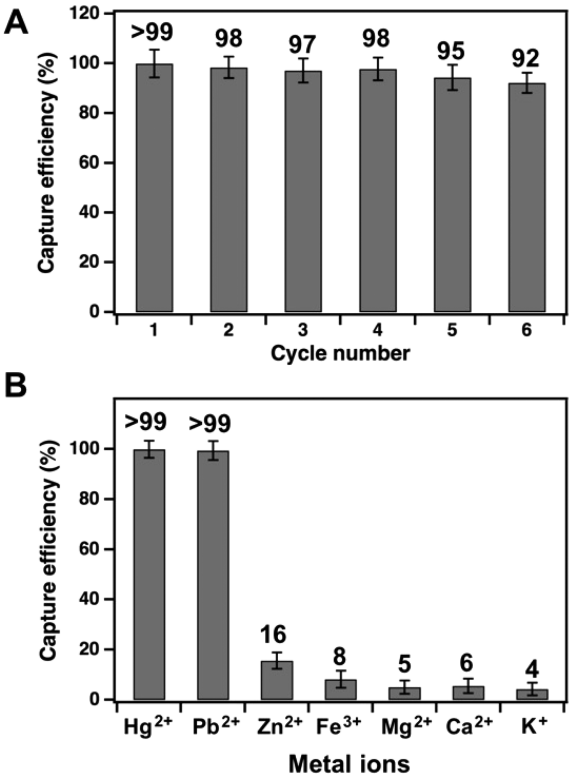

Figure 6. (A) Cycle performance for Hg(II) removal in aqueous solution. (B) Capture efficiency in removing metal ions.

materials, such as Cr-MIL-101s,[11m] mesoporous silicas,[11h] and porous carbons,[11g] which eventually lose their capacity upon cycle. In addition, the Hg(II)-loaded TAPB-BMTTPA-COF still retain high crystallinity (Figure S9). Selectivity is an another important factor for practical Hg(II) removal from water. As shown in Figure 6B, TAPB-BMTTPA-COF can effectively remove toxic heavy metal ions, such as Hg(II) and Pb(II), but it is not active for other metal ions, such as Zn(II), Fe(III), Mg(II), Ca(II), and K(I). Therefore, TAPB-BMTTPA-COF is able to remove toxic metal ions in a highly selective manner. In the mixture solution of Hg(II), Zn(II), Fe(III), Mg(II), Ca(II), and K(I) ions at each concentration of 10 ppm at pH = 7, the TAPB-BMTTPA-COF still retains high efficiency for Hg(II) and Pb(II) ions (Figure S9).

Adsorption Mechanism. In order to investigate the mechanism for the highly effective capture of Hg(II), we utilized ^{13}C CP/MAS NMR and fluorescent emission spectrum to evaluate the interaction between Hg(II) and TAPB-BMTTPA-COF. Solid-state ^{13}C cross-polarization magic-angle spinning (CP/MAS) NMR spectroscopy provided a solid body of evidence to support the strong interaction between Hg(II) and the S atoms. The ^{13}C CP/MAS NMR spectrum of TAPB-BMTTPA-COF is shown in Figure 7 (black curve), the signals at 17 and 147 ppm, which are ascribed to the methyl carbon adjacent to the S atoms and the imine-bond carbon in TAPB-BMTTPA-COF, respectively. Upon the capture of Hg(II), the methyl carbon signal was downfield shifted to 26 ppm (Figure 7, blue curve), while the imine-bond carbon and other signals were almost unchanged. This result reveals the soft methylthio

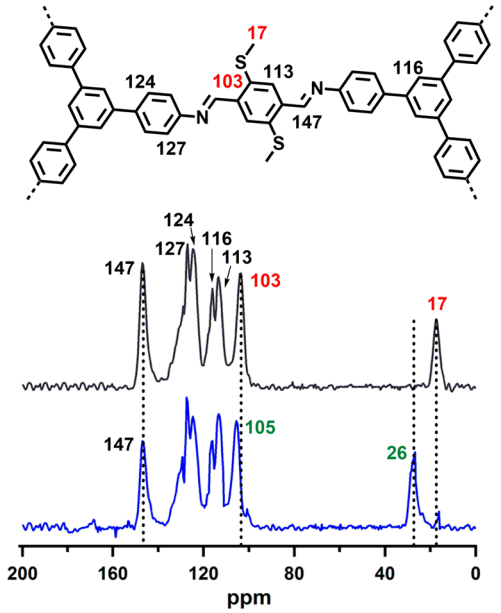

Figure 7. ^{13}C CP/MAS NMR spectra of TAPB-BMTTPA-COF (black curve) and Hg(II)-adsorbed TAPB-BMTTPA-COF (blue curve).

groups bond with preference with soft heavy Hg(II) ions, whereas the imine bond plays a little role in the Hg(II) capture.

The coordination interactions between Hg(II) and methylthio units in TAPB-BMTTPA-COF were also verified by electronic absorption spectroscopic measurements (K/M spectra). The solid samples of TAPB-BMTTPA-COF exhibited an adsorption band at 477 nm (Figure S10, black curve). After adsorption of Hg(II), the solid TAPB-BMTTPA-COF sample exhibited the same B-band at 477 nm accompanied by a new strong band at 605 nm (Figure S10, red curve), which was generated by the charge transfer from the electron-rich methylthio group to electron-deficient Hg(II) metal ions. In addition, the charge-transfer interaction between the TAPB-BMTTPA-COF and Hg(II) ions triggered the quenching of fluorescence emission. The pristine TAPB-BMTTPA-COF sample features a broad emission centered at 534 nm (Figure S11, black curve). After the adsorption of Hg(II), the intensity was decreased to a level of less than 8% of the original one (red curve). Therefore, the effective capture of Hg(II) by TAPB-BMTTPA-COF stems essentially from the interactions between Hg(II) and the S atoms.

The sulfur-free imine-linked TPB-DMTP-COF[6b] was employed as control sample to investigate the contribution of the imine donors in the uptake of Hg(II) and Pb(II). Under the same conditions, the TPB-DMTP-COF adsorbed only 5% Hg(II) and 2% Pb(II) from the aqueous solutions. This result also indicates that the imine donors in the COF materials contribute little to the capture of Hg(II) and Pb(II).

CONCLUSIONS

Porous materials are promising for removing toxic heavy metal ions from water; however, a suitable material requires systematic control over stability, porosity, pore walls, and pore environments, which is still challenging for most porous materials. COFs are unique in that they combine high stability, large porosity, dense functional units, and high accessibility of active sites through the rational design of skeletons and pores. With these elegant features, COFs achieve unprecedented high

DOI: 10.1021/jacs.6b12328
J. Am. Chem. Soc. 2017, 139, 2428−2434

performance in removing Hg(II) from aqueous solutions by achieving capacity, efficiency, effectivity, durability over a wide pH range, selectivity, and reusability. These results set a new benchmark for removing toxic metals and suggest the great potential of COFs for challenging various pollution issues.

■ ASSOCIATED CONTENT

Supporting Information

The Supporting Information is available free of charge on the ACS Publications website at DOI: 10.1021/jacs.6b12328.

Materials and methods, syntheses and characterizations, Tables S1−S5, and Figures S1−S6 (PDF)

■ AUTHOR INFORMATION

Corresponding Author

*djiang@jaist.ac.jp

ORCID

Donglin Jiang: 0000-0002-3785-1330

Author Contributions

†N.H. and L.Z. contributed equally.

Notes

The authors declare no competing financial interest.

■ REFERENCES

(1) (a) Feng, X.; Ding, X.; Jiang, D. *Chem. Soc. Rev.* **2012**, *41*, 6010−6022. (b) Waller, P. J.; Gándara, F.; Yaghi, O. M. *Acc. Chem. Res.* **2015**, *48*, 3053−3063. (c) Ding, S.-Y.; Wang, W. *Chem. Soc. Rev.* **2013**, *42*, 548−568. (d) Colson, J. W.; Dichtel, W. R. *Nat. Chem.* **2013**, *5*, 453−465. (e) Huang, N.; Wang, P.; Jiang, D. *Nat. Rev. Mater.* **2016**, *1*, 16068. (f) Doonan, C. J.; Tranchemontagne, D. J.; Glover, T. G.; Hunt, J. R.; Yaghi, O. M. *Nat. Chem.* **2010**, *2*, 235−238. (g) Liu, Y.; Ma, Y.; Zhao, Y.; Sun, X.; Gándara, F.; Furukawa, H.; Liu, Z.; Zhu, H.; Zhu, C.; Suenaga, K.; Oleynikov, P.; Alshammari, A. S.; Zhang, X.; Terasaki, O.; Yaghi, O. M. *Science* **2016**, *351*, 365−369. (h) DeBlase, C. R.; Dichtel, W. R. *Macromolecules* **2016**, *49*, 5297−5305.

(2) (a) Côté, A. P.; Benin, A. I.; Ockwig, N. W.; O'Keeffe, M.; Matzger, A. J.; Yaghi, O. M. *Science* **2005**, *310*, 1166−1170. (b) Ding, X.; Chen, L.; Honsho, Y.; Feng, X.; Saengsawang, O.; Guo, J.; Saeki, A.; Seki, S.; Irle, S.; Nagase, S.; Parasuk, V.; Jiang, D. *J. Am. Chem. Soc.* **2011**, *133*, 14510−14513. (c) El-Kaderi, H. M.; Hunt, J. R.; Mendoza-Cortés, J. L.; Côté, A. P.; Taylor, R. E.; O'Keeffe, M.; Yaghi, O. M. *Science* **2007**, *316*, 268−272. (d) Rabbani, M. G.; Sekizkardes, A. K.; Kahveci, Z.; Reich, T. E.; Ding, R.; El-Kaderi, H. M. *Chem. - Eur. J.* **2013**, *19*, 3324−3328. (e) Zhou, T.-Y.; Xu, S.-Q.; Wen, Q.; Pang, Z.-F.; Zhao, X. *J. Am. Chem. Soc.* **2014**, *136*, 15885−15888. (f) Huang, N.; Ding, X.; Kim, J.; Ihee, H.; Jiang, D. *Angew. Chem., Int. Ed.* **2015**, *54*, 8704−8707. (g) Dalapati, S.; Addicoat, M.; Jin, S.; Sakurai, T.; Gao, J.; Xu, H.; Irle, S.; Seki, S.; Jiang, D. *Nat. Commun.* **2015**, *6*, 7786. (h) Zhu, Y.; Wan, S.; Jin, Y.; Zhang, W. *J. Am. Chem. Soc.* **2015**, *137*, 13772−13775. (i) Ascherl, L.; Sick, T.; Margraf, J. T.; Lapidus, S. H.; Calik, M.; Hettstedt, C.; Karaghiosoff, K.; Döblinger, M.; Clark, T.; Chapman, K. W.; Auras, F.; Bein, T. *Nat. Chem.* **2016**, *8*, 310−316. (j) Pang, Z.-F.; Xu, S.-Q.; Zhou, T.-Y.; Liang, R.-R.; Zhan, T.-G.; Zhao, X. *J. Am. Chem. Soc.* **2016**, *138*, 4710−4713.

(3) (a) Dalapati, S.; Jin, S.; Gao, J.; Xu, Y.; Nagai, A.; Jiang, D. *J. Am. Chem. Soc.* **2013**, *135*, 17310−17313. (b) Fang, Q.; Zhuang, Z.; Gu, S.; Kaspar, R. B.; Zheng, J.; Wang, J.; Qiu, S.; Yan, Y. *Nat. Commun.* **2014**, *5*, 4503. (c) Uribe-Romo, F. J.; Hunt, J. R.; Furukawa, H.; Klöck, C.; O'Keeffe, M.; Yaghi, O. M. *J. Am. Chem. Soc.* **2009**, *131*, 4570−4571. (d) Stegbauer, L.; Schwinghammer, K.; Lotsch, B. V. *Chem. Sci.* **2014**, *5*, 2789−2793. (e) Du, Y.; Yang, H.; Whiteley, J. M.; Wan, S.; Jin, Y.; Lee, S.-H.; Zhang, W. *Angew. Chem., Int. Ed.* **2016**, *55*, 1737−1741. (f) Zhuang, X.; Zhao, W.; Zhang, F.; Cao, Y.; Liu, F.; Bi, S.; Feng, X. *Polym. Chem.* **2016**, *7*, 4176−4181. (g) El-Kaderi, H. M.; Hunt, J. R.; Mendoza-Cortés, J. L.; Côté, A. P.; Taylor, R. E.; O'Keeffe, M.; Yaghi, O. M. *Science* **2007**, *316*, 268−272. (h) Liu, Y.; Ma, Y.; Zhao, Y.; Sun, X.; Gándara, F.; Furukawa, H.; Liu, Z.; Zhu, H.; Zhu, C.; Suenaga, K.; Oleynikov, P.; Alshammari, A. S.; Zhang, X.; Terasaki, O.; Yaghi, O. M. *Science* **2016**, *351*, 365−369.

(4) (a) Chen, L.; Furukawa, K.; Gao, J.; Nagai, A.; Nakamura, T.; Dong, Y.; Jiang, D. *J. Am. Chem. Soc.* **2014**, *136*, 9806−9809. (b) Jin, S.; Supur, M.; Addicoat, M.; Furukawa, K.; Chen, L.; Nakamura, T.; Fukuzumi, S.; Irle, S.; Jiang, D. *J. Am. Chem. Soc.* **2015**, *137*, 7817−7827. (c) Calik, M.; Auras, F.; Salonen, L. M.; Bader, K.; Grill, I.; Handloser, M.; Medina, D. D.; Dogru, M.; Löbermann, F.; Trauner, D.; Hartschuh, A.; Bein, T. *J. Am. Chem. Soc.* **2014**, *136*, 17802−17807. (d) Dogru, M.; Handloser, M.; Auras, F.; Kunz, T.; Medina, D.; Hartschuh, A.; Knochel, P.; Bein, T. *Angew. Chem., Int. Ed.* **2013**, *52*, 2920−2924.

(5) (a) Wan, S.; Guo, J.; Kim, J.; Ihee, H.; Jiang, D. *Angew. Chem., Int. Ed.* **2008**, *47*, 8826−8830. (b) Wan, S.; Guo, J.; Kim, J.; Ihee, H.; Jiang, D. *Angew. Chem., Int. Ed.* **2009**, *48*, 5439−5442. (c) Ding, S.-Y.; Dong, M.; Wang, Y.-W.; Chen, Y.-T.; Wang, H.-Z.; Su, C.-Y.; Wang, W. *J. Am. Chem. Soc.* **2016**, *138*, 3031−3037. (d) Dalapati, S.; Jin, E.; Addicoat, M.; Heine, T.; Jiang, D. *J. Am. Chem. Soc.* **2016**, *138*, 5797−5800.

(6) (a) Ding, S.-Y.; Gao, J.; Wang, Q.; Zhang, Y.; Song, W.-G.; Su, C.-Y.; Wang, W. *J. Am. Chem. Soc.* **2011**, *133*, 19816−19822. (b) Xu, H.; Gao, J.; Jiang, D. *Nat. Chem.* **2015**, *7*, 905−912. (c) Shinde, D. B.; Kandambeth, S.; Pachfule, P.; Kumar, R. R.; Banerjee, R. *Chem. Commun.* **2015**, *51*, 310−313. (d) Stegbauer, L.; Schwinghammer, K.; Lotsch, B. V. *Chem. Sci.* **2014**, *5*, 2789−2793. (e) Fang, Q.; Gu, S.; Zheng, J.; Zhuang, Z.; Qiu, S.; Yan, Y. *Angew. Chem., Int. Ed.* **2014**, *53*, 2878−2882. (f) Vyas, V. S.; Haase, F.; Stegbauer, L.; Savasci, G.; Podjaski, F.; Ochsenfeld, C.; Lotsch, B. V. *Nat. Commun.* **2015**, *6*, 8508. (g) Xu, H.-S.; Ding, S.-Y.; An, W.-K.; Wu, H.; Wang, W. *J. Am. Chem. Soc.* **2016**, *138*, 11489−11492. (h) Wang, X.; Han, X.; Zhang, J.; Wu, X.; Liu, Y.; Cui, Y. *J. Am. Chem. Soc.* **2016**, *138*, 12332−12335.

(7) (a) Chandra, S.; Kundu, T.; Dey, K.; Addicoat, M.; Heine, T.; Banerjee, R. *Chem. Mater.* **2016**, *28*, 1489−1494. (b) Chandra, S.; Kundu, T.; Kandambeth, S.; BabaRao, R.; Marathe, Y.; Kunjir, S. M.; Banerjee, R. *J. Am. Chem. Soc.* **2014**, *136*, 6570−6573. (c) Xu, H.; Tao, S.; Jiang, D. *Nat. Mater.* **2016**, *15*, 722−726. (d) Ma, H.; Liu, B.; Li, B.; Zhang, L.; Li, Y.-G.; Tan, H.-Q.; Zang, H.-Y.; Zhu, G. *J. Am. Chem. Soc.* **2016**, *138*, 5897−5903.

(8) (a) DeBlase, C. R.; Silberstein, K. E.; Truong, T.-T.; Abruña, H. D.; Dichtel, W. R. *J. Am. Chem. Soc.* **2013**, *135*, 16821−16824. (b) Wang, C.; Liao, H.; Wang, H.; Ding, H.; Meng, X.; Xu, H.; Wang, B.; Ai, X. *J. Mater. Chem. A* **2016**, *4*, 7416−7421. (c) Xu, F.; Jin, S.; Zhong, H.; Wu, D.; Yang, X.; Chen, X.; Wei, H.; Fu, R.; Jiang, D. *Sci. Rep.* **2015**, *5*, 8225. (d) Xu, F.; Xu, H.; Chen, X.; Wu, D.; Wu, Y.; Liu, H.; Gu, C.; Fu, R.; Jiang, D. *Angew. Chem., Int. Ed.* **2015**, *54*, 6814−6818. (e) Mulzer, C. R.; Shen, L.; Bisbey, R. P.; McKone, J. R.; Zhang, N.; Abruña, H. D.; Dichtel, W. R. *ACS Cent. Sci.* **2016**, *2*, 667−673. (f) DeBlase, C. R.; Hernández-Burgos, K.; Rotter, J. M.; Fortman, D. J.; Abreu, D. S.; Timm, R. A.; Diógenes, I. C. N.; Kubota, L. T.; Abruña, H. D.; Dichtel, W. R. *Angew. Chem., Int. Ed.* **2015**, *54*, 13225−13229.

(9) (a) Huang, N.; Chen, X.; Krishna, R.; Jiang, D. *Angew. Chem., Int. Ed.* **2015**, *54*, 2986−2990. (b) Huang, N.; Krishna, R.; Jiang, D. *J. Am. Chem. Soc.* **2015**, *137*, 7079−7082. (c) Kang, Z.; Peng, Y.; Qian, Y.; Yuan, D.; Addicoat, M. A.; Heine, T.; Hu, Z.; Tee, L.; Guo, Z.; Zhao, D. *Chem. Mater.* **2016**, *28*, 1277−1285. (d) Stegbauer, L.; Hahn, M. W.; Jentys, A.; Savasci, G.; Ochsenfeld, C.; Lercher, J. A.; Lotsch, B. V. *Chem. Mater.* **2015**, *27*, 7874−7881.

(10) (a) McNutt, M. *Science* **2013**, *341*, 1430. (b) Atwood, D. A.; Zaman, M. K. *Struct. Bonding (Berlin)* **2006**, *120*, 163−182. (c) Shin, Y.; Fryxell, G. E.; Um, W.; Parker, K.; Mattigod, S. V.; Skaggs, R. *Adv. Funct. Mater.* **2007**, *17*, 2897−2901. (d) Huang, C. P.; Blankenship, D. W. *Water Res.* **1984**, *18*, 37−46. (e) Blanchard, G.; Maunaye, M.; Martin, G. *Water Res.* **1984**, *18*, 1501−1507. (f) Benhammou, A.; Yaacoubi, A.; Nibou, L.; Tanouti, B. *J. Colloid Interface Sci.* **2005**, *282*, 320−326. (g) Xu, Y.; Jin, S.; Xu, H.; Nagai, A.; Jiang, D. *Chem. Soc. Rev.* **2013**, *42*, 8012−8031.

DOI: 10.1021/jacs.6b12328
J. Am. Chem. Soc. 2017, 139, 2428−2434

(11) (a) Fang, Q.-R.; Yuan, D.-Q.; Sculley, J.; Li, J.-R.; Han, Z.-B.; Zhou, H.-C. *Inorg. Chem.* **2010**, *49*, 11637−11642. (b) He, J.; Yee, K.-K.; Xu, Z.; Zeller, M.; Hunter, A. D.; Chui, S. S.-Y.; Che, C.-M. *Chem. Mater.* **2011**, *23*, 2940−2947. (c) Ding, S.-Y.; Dong, M.; Wang, Y.-W.; Chen, Y.-T.; Wang, H.-Z.; Su, C.-Y.; Wang, W. *J. Am. Chem. Soc.* **2016**, *138*, 3031−3037. (d) Bebout, D. C. Mercury: Inorganic & Coordination Chemistry. In *Encyclopedia of Inorganic and Bioinorganic Chemistry*; John Wiley & Sons, Ltd.: New York, 2011. (e) Yee, K.-K.; Reimer, N.; Liu, J.; Cheng, S.-Y.; Yiu, S.-M.; Weber, J.; Stock, N.; Xu, Z. *J. Am. Chem. Soc.* **2013**, *135*, 7795−7798. (f) Luo, F.; Chen, J. L.; Dang, L. L.; Zhou, W. N.; Lin, H. L.; Li, J. Q.; Liu, S. J.; Luo, M. B. *J. Mater. Chem. A* **2015**, *3*, 9616−9620. (g) Shin, Y.; Fryxell, G. E.; Um, W.; Parker, K.; Mattigod, S. V.; Skaggs, R. *Adv. Funct. Mater.* **2007**, *17*, 2897−2901. (h) Liu, J.; Feng, X.; Fryxell, G. E.; Wang, L.-Q.; Kim, A. Y.; Gong, M. *Adv. Mater.* **1998**, *10*, 161−165. (i) Bag, S.; Trikalitis, P. N.; Chupas, P. J.; Armatas, G. S.; Kanatzidis, M. G. *Science* **2007**, *317*, 490−493. (j) Yantasee, W.; Warner, C. L.; Sangvanich, T.; Addleman, R. S.; Carter, T. G.; Wiacek, R. J.; Fryxell, G. E.; Timchalk, C.; Warner, M. G. *Environ. Sci. Technol.* **2007**, *41*, 5114−5119. (k) Manos, M. J.; Petkov, V. G.; Kanatzidis, M. G. *Adv. Funct. Mater.* **2009**, *19*, 1087−1092. (l) Li, B.; Zhang, Y.; Ma, D.; Shi, Z.; Ma, S. *Nat. Commun.* **2014**, *5*, 5537. (m) Liu, T.; Che, J.-X.; Hu, Y.-Z.; Dong, X.-W.; Liu, X.-Y.; Che, C.-M. *Chem. - Eur. J.* **2014**, *20*, 14090−14095.

(12) Yamamoto, T.; Nishimura, T.; Mori, T.; Miyazaki, E.; Osaka, I.; Takimiya, K. *Org. Lett.* **2012**, *14*, 4914−4917.

DOI: 10.1021/jacs.6b12328
J. Am. Chem. Soc. 2017, 139, 2428−2434